

On the pathways of the equatorial subsurface currents in the eastern equatorial Pacific and their contributions to the Peru-Chile Undercurrent

Ivonne Montes,^{1,2} Francois Colas,³ Xavier Capet,⁴ and Wolfgang Schneider^{2,5}

Received 11 August 2009; revised 19 February 2010; accepted 12 April 2010; published 3 September 2010.

[1] The connections between the Equatorial Current System and the Peru Current System in the eastern tropical Pacific (ETP) are examined with a primitive equations eddy-resolving regional model. The quasi-equilibrium solutions reproduce three eastward equatorial subsurface currents of interest: the Equatorial Undercurrent (EUC, located between 1°N and 1°S), the primary Southern Subsurface Countercurrent (pSSCC, between 3° and 4°S) and, farther south the secondary Southern Subsurface Countercurrent (sSSCC, between 7° and 8°S). Using a Lagrangian tracking procedure, the fate of these currents in the ETP and their contribution to the Peru-Chile Undercurrent (PCUC) are studied. Lagrangian diagnostics show that for the most part the EUC water contributes to westward flows, including the South Equatorial Current and deeper flows below it, and strikingly only a very little fraction feeds the PCUC, while a significant part of both SSCCs contribute substantially. Mesoscale eddies are shown to exert an effect on these connections. In addition, about 30% of the PCUC is fed by the three subsurface equatorial flows (EUC, pSSCC, sSSCC). The remaining part of the PCUC comes from an alongshore recirculation associated with flows below it, and from the southern part of the domain (south of ~9°S).

Citation: Montes, I., F. Colas, X. Capet, and W. Schneider (2010), On the pathways of the equatorial subsurface currents in the eastern equatorial Pacific and their contributions to the Peru-Chile Undercurrent, *J. Geophys. Res.*, 115, C09003, doi:10.1029/2009JC005710.

1. Introduction

[2] Several studies based on Eulerian measurements, geostrophic flow estimates, and Ocean General Circulation Models (OGCMs) were carried out in order to understand the circulation patterns of the Eastern Tropical Pacific [Kessler, 2006]. This oceanic region delimited by the 120°W parallel and the west coast of South America hosts two important current systems. The Equatorial Current System [Cromwell *et al.*, 1954; Wyrtki, 1963, 1967; Tsuchiya, 1975; Lukas, 1986; Johnson and Moore, 1997; Johnson and McPhaden, 1999; McCreary *et al.*, 2002] is composed of quasi zonal currents: the Equatorial Undercurrent (EUC) and the primary and secondary Southern Subsurface Countercurrents (pSSCC and sSSCC) which flow eastward in the subsurface; and the South Equatorial Current (SEC) which flows westward near

the surface. The other major system, the Peru Current system [Gunther, 1936; Brockmann *et al.*, 1980; Tsuchiya, 1985; Huyer *et al.*, 1991; Strub *et al.*, 1998], is composed of currents that are strongly influenced by the presence of the south American landmass: the Peru Coastal Current (PCC) and the Peru Oceanic Current (POC) near the surface; the Peru-Chile Countercurrent (PCCC) and the Peru-Chile Undercurrent (PCUC) in the subsurface. Figure 1 schematically represents these various currents.

[3] Combined studies of these two systems have revealed important connections between them which can be anticipated from the fact that, upon reaching the American landmass, eastward equatorial currents must recirculate, or merge with or feed other currents. For example, Wyrtki [1963], Lukas [1986], Blanke and Raynaud [1997], and Strub *et al.* [1998] indicate that part of the upper EUC upwells into the SEC. On the other hand, its lower layers are thought to be probably an important source of the water carried by the PCUC [Wyrtki, 1963; Brink *et al.*, 1983; Lukas, 1986; Toggweiler *et al.*, 1991; Fiedler and Talley, 2006]. It has also been suggested that both SSCCs could be complementary sources of PCUC water [Lukas, 1986; Toggweiler *et al.*, 1991]. Such connections are certainly modified during active phases of El Niño during which substantial amounts of equatorial water are being advected along the Peruvian coast as far as 15–20°S [Colas *et al.*, 2008; Kessler, 2006, and references therein]. However, existing data sets are too sparse (in space and time) to quantify these connections. As

¹Programa de Postgrado en Oceanografía, Departamento de Oceanografía, Universidad de Concepción, Concepción, Chile.

²Centro de Investigación Oceanográfica en el Pacífico Sur-Oriental, Universidad de Concepción, Concepción, Chile.

³Institute of Geophysics and Planetary Physics, University of California, Los Angeles, California, USA.

⁴Laboratoire de Physique des Océans, UMR 6523, UBO, CNRS, IFREMER, IRD, Plouzane, France.

⁵Departamento de Oceanografía, Universidad de Concepción, Concepción, Chile.

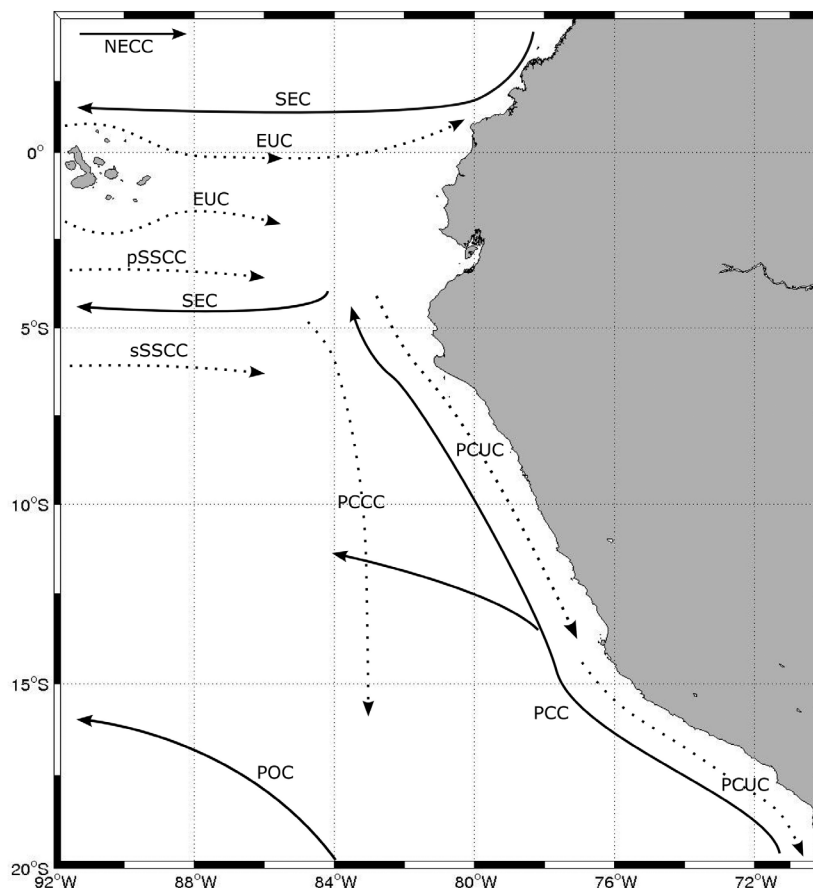


Figure 1. Oceanic circulation scheme for the eastern tropical Pacific, compiled from *Gunther* [1936], *Wyrski* [1963], *Tsuchiya* [1975,1985], *Lukas* [1986], *Huyer et al.* [1991], *Strub et al.* [1998], *Johnson and McPhaden* [1999], *Rowe et al.* [2000], *McCreary et al.* [2002], and *Kessler* [2006]. Solid lines indicate surface currents and dotted lines show subsurface currents. NECC: North Equatorial Countercurrent; SEC: South Equatorial Current; EUC: Equatorial Undercurrent; pSSCC: primary Southern Subsurface Countercurrent; sSSCC: secondary Southern Subsurface Countercurrent; PCC: Peru Coastal Current; POC: Peru Oceanic Current; PCUC: Peru-Chile Undercurrent; and PCCC: Peru-Chile Countercurrent.

for OGCMs, with coarse resolution of the order of 1 degree, the subsurface currents of interest that do not exceed a width of 2 degrees in latitude are poorly resolved. Hence, the study of water pathways related to these currents is somewhat limited considering that the interactions with the Equatorial and the Peru Current System take place within a roughly 10×10 degrees region. The question of the connections between equatorial and extra-equatorial oceanic regions is an important one, in particular for its implications on climate and also ecosystems [*Lavin et al.*, 2006; *Chavez et al.*, 2008].

[4] Our study considers the connections between the Equatorial and Peruvian current systems in Primitive Equations eddy-resolving numerical solutions (based on the configuration developed and validated by *Penven et al.* [2005], presented in section 2.1) over a domain that encompasses the eastern equatorial and Peruvian systems. Precisely, we rely on the (offline) calculation of thousands of Lagrangian trajectories for these solutions (see section 2.2). The numerical floats are released at strategic locations within the equatorial subsurface counter currents and the PCUC and tracked either forward or backward in time. This allows us to quantify the main exchanges that take place in the eastern Pacific and to

assess the role of the eddies (section 3) in these exchanges. Most importantly, we find that the PCUC carries a water mixture composed for about a third by EUC, pSSCC and sSSCC water (the former having a small contribution). We also find that mesoscale eddies exert a noticeable effect in particular on the SSCCs/PCUC and sSSCC/SEC connections.

[5] Assessing the degree of uncertainty in the equatorial subsurface pathways and PCUC water sources is difficult. The primary reason is that it is not straightforward to translate the Eulerian biases (which are only approximately known given the limited amount of observational data) into Lagrangian biases. We limit our study to a basic check that the Lagrangian results are not overly sensitive to the underlying Eulerian field. To do so, two numerical solutions that correspond to two different sets of lateral boundary conditions are computed (see section 2.1).

2. Methodology

2.1. Eulerian Solutions

[6] The numerical quasi-equilibrium solutions we analyze were obtained with ROMS (for a complete description of the

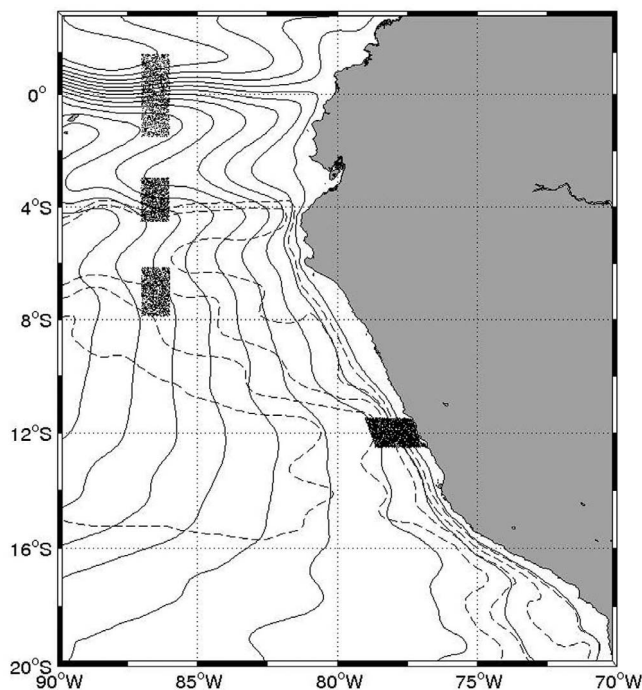


Figure 2. Map showing the model domain, the stream function derived from annual mean velocities at 100 m depth (solid line) and at 170 m depth (dashed line) of the ROccam solution and, the initial position of floats identified as part of each equatorial subsurface current (between 86°W and 87°W) and the Peru - Chile Undercurrent (PCUC cross-shore section). Each equatorial group is composed of 36000 floats integrated forward in time for 2 climatological years and distributed evenly between 40 and 250 m depth. The PCUC floats are composed of 3809 floats distributed evenly between 30 and 400 m depth and integrated backward in time for 3 climatological years. The horizontal flow was decomposed into an irrotational and a nondivergent component applying the Helmholtz theorem from which a stream function representative of the nondivergent flow was obtained. For details see *Penven et al. [2005]*.

model, see *Shchepetkin and McWilliams [2003, 2005]*) using the model configuration developed by *Penven et al. [2003, 2005]*. The corresponding solution that we call ROccam is forced by climatological conditions at lateral boundaries and air-sea interface. The domain covered by ROccam spans the region between 3°N and 20°S and between 70°W and 90°W . The horizontal model resolution is $1/9^{\circ}$ (~ 12 km) with 32 vertical levels. The topography is derived from a $2'$ resolution database [*Smith and Sandwell, 1997*]. The model is forced with heat fluxes and fresh water fluxes from the COADS ocean surface monthly climatology [*Da Silva et al., 1994*]. For wind stress, a monthly mean climatology is computed from QuikSCAT satellite scatterometer data [*Liu et al., 1998*]. The three lateral open boundaries are forced using a climatology derived from the Ocean Circulation and Advanced Modelling Project (OCCAM) global ocean model at $1/4^{\circ}$ resolution [*Saunders et al., 1999*]. (The OCCAM model was forced by an annual cycle of monthly winds from the years 1986–1988 of the ECMWF model. For the initial-

ization was used the potential temperature and salinity field from the Levitus'94 annual mean climatology.) The simulations were performed over a 16-year period, during which 3-day averages of the model output were stored. The model solution reached a statistical equilibrium (in terms of upper ocean stratification and eddy kinetic energy levels) by year 3. The first 3 years were consequently discarded as the spin up phase (for details of the spin-up procedure please refer to *Penven et al. [2005]*). *Penven et al. [2003, 2005]* evaluated the mean circulation and thermohaline structure, their seasonal cycle, and the meso-scale activity. They showed that the known aspects of the regional dynamics are adequately reproduced by ROMS quasi-equilibrium climatological solutions [see *Penven et al., 2005, Figure 2*].

[7] The questions we wish to investigate involve basin scale currents that are primarily passed on to our regional model through the lateral boundary conditions. The sensitivity to these boundary conditions is assessed by performing an additional simulation (called RSoda) which is identical to ROccam in every aspect but the open boundary conditions, derived from a climatology of the SODA global ocean reanalysis at $1/2^{\circ}$ resolution [*Carton and Giese, 2008*]. (SODA was forced by ERA-40 surface fluxes [*Uppala et al., 2005*], and constrained by data assimilation in situ and satellite altimetric data.) The temperature, salinity and velocity fields for the northern, western and southern open boundaries used in ROccam and RSoda are shown by V. Echevin et al. (personal communication, 2009), and their differences are discussed therein.

2.2. Lagrangian Analysis

[8] A ROMS-offline tracking module is used to calculate numerical Lagrangian (float) trajectories from stored ROMS velocity fields [*Carr et al., 2008; Capet et al., 2004*]. The floats are supposed to be neutrally buoyant and are advected either forward or backward in time by the 3-day average velocity field linearly interpolated at floats locations (unless otherwise stated, velocities are 3-day accumulated averages). This kind of numerical Lagrangian approach has proved to be an appropriate method for studying the origin and the fate of ocean water masses [e.g., *Blanke et al., 2002*].

[9] We perform two different types of experiments. The first one consists in launching in the 11th and 12th year of simulation 3 groups of floats into each equatorial subsurface current and integrating these forward in time for 2 years. Each group is composed of 1500 floats released each month starting in January and ending in December (36000 in total), and distributed randomly (using a uniform distribution yields identical results) between ~ 40 m and 250 m depth and bounded between 1.5°N – 1.5°S and 86°W – 87°W (EUC), 3°S – 4.5°S and 86°W – 87°W (pSSCC), and 6.25°S – 7.75°S and 86°W – 87°W (sSSCC), respectively (Figures 2 and 3). These boundaries correspond to the geographic ranges (longitude, latitude, and depth) of equatorial subsurface counter currents derived from the model Eulerian outputs (see section 3.1). (ROccam and RSoda exhibit a slightly different vertical structure of equatorial subsurface currents. Therefore, in Figure 3b, the initial float release areas in the EUC and sSSCC were adjusted in RSoda to match the observed currents.) Criteria used to associate a float to a specific current are further described in section 3.2.1.

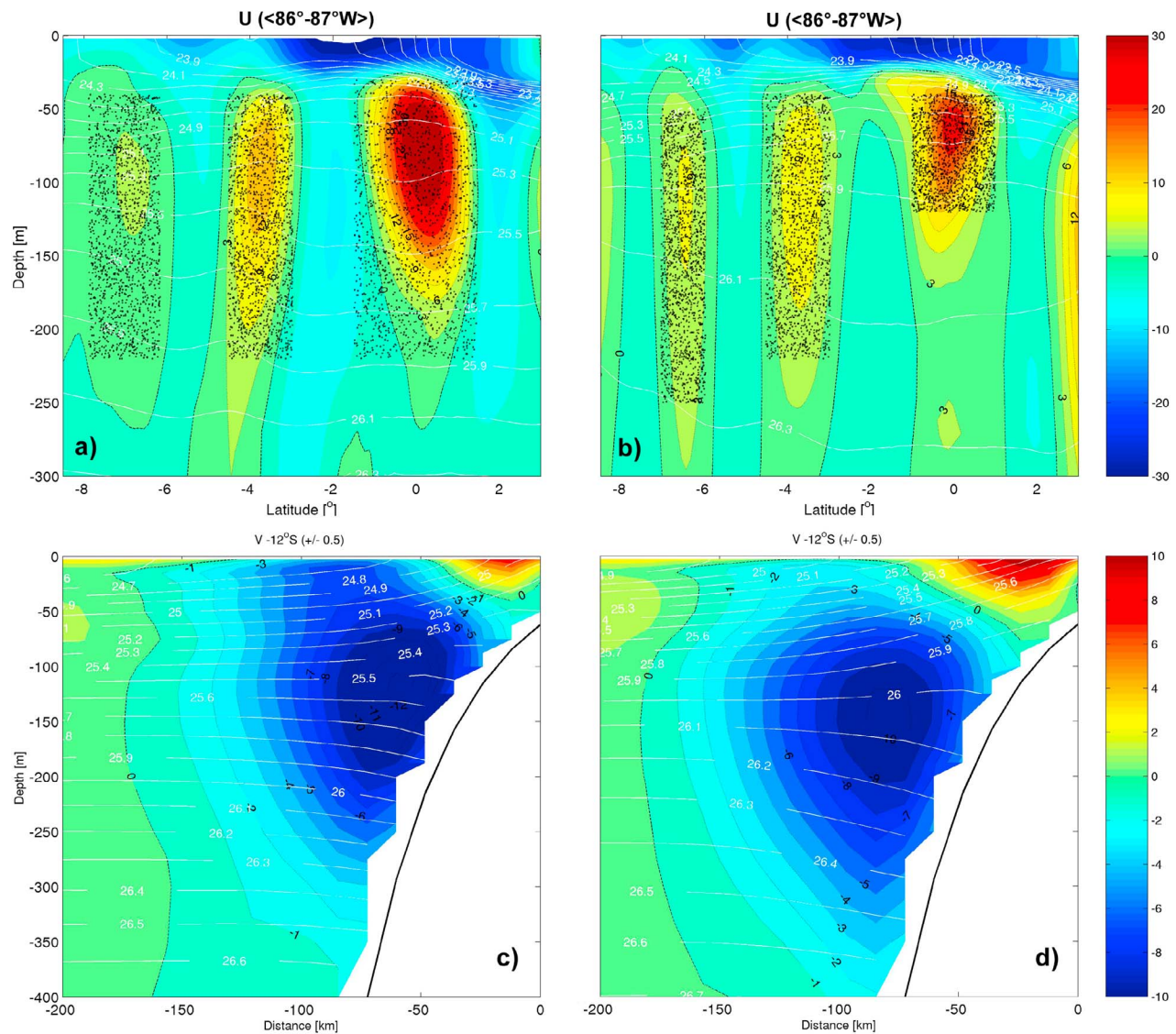


Figure 3. Vertical sections of annual mean zonal velocity (cm s^{-1}) averaged between 86°W and 87°W and, generated from (a) ROccam, (b) RSoda, and annual mean meridional velocity (cm s^{-1}) averaged over 11.5°S – 12.5°S generated from (c) ROccam and (d) RSoda showing the vertical structure of the Equatorial Current System and the Peruvian Current System, respectively. Zonal and meridional velocities are color shaded (the color bars on the right-hand side relate colors to velocity in cm s^{-1}) and eastward zonal velocities (Figures 3a and 3b) and poleward meridional velocities (Figures 3c and 3d) are contoured with black dotted lines; selected contours are marked with their respective magnitude. Density ($\sigma\text{-t}$ in kg m^{-3}) is depicted as white contour lines. The launch positions, in the forward experiment, are shown with black dots.

[10] The second experiment consists in releasing a larger number of floats (3809) randomly distributed on a vertical section in the PCUC and integrating them backward in time for 3 climatological years. We choose a cross-shore section, with depths from 30 m to 400 m, located between 11.5°S and 12.5°S and from the coast until 79°W to represent the PCUC (Figure 2). The criterion to identify properly all floats hosted on the PCUC is described in section 3.2.3.

[11] Each of these experiments is carried out with the 3-day average velocities from ROccam and RSoda. In addition, the forward tracking experiment is also performed using seasonally averaged velocity fields from ROccam. This allows

us to identify the eddy contribution to the water transport between the Equatorial and Peruvian current systems.

3. Regional Connections Between the Current Systems: Results and Discussion

3.1. Eulerian Structure: Equatorial Current System and Peru Current System

[12] First, we check that the numerical simulations capture the currents of interest. To do so, we extracted vertical sections of the annual mean zonal and meridional velocity from ROMS solutions (Figure 3). Figures 3a and 3b present the

vertical structure of velocity from 3°N to 8.5°S averaged between 86°W and 87°W, just east of the Galapagos Islands, for both simulations: ROccam and RSoda, respectively. The three principal subsurface counter currents and the westward surface current (South Equatorial Current – SEC, in dark and light blue colors) as described by *Cromwell et al.* [1954], *Lukas* [1986], *Tsuchiya* [1975, 1985], *Johnson and Moore* [1997], *Rowe et al.* [2000], *McCreary et al.* [2002], *Donohue et al.* [2002], and *Kessler* [2006], which constitute the Equatorial Current System are clearly reproduced in both simulations, although different in strength and vertical extension. The northernmost subsurface current, extends from about 30–200 m depth in both simulations, is located between 1.5°N and 1.5°S, and corresponds to the EUC after flowing around the Galapagos Islands. It flows eastward with maximum mean velocities of 20–30 cm s⁻¹, being more pronounced and stronger in ROccam. The second and third, from north to south, subsurface currents are located between 3°–4.5°S and 6°–8°S, corresponding to the primary and secondary Southern Subsurface Countercurrents, pSSCC and sSSCC, respectively. Both in ROccam and RSoda, these eastward currents flow with maximum mean velocities of about 5 cm s⁻¹ to 15 cm s⁻¹ in their cores, but nevertheless the sSSCC is much weaker in ROccam.

[13] Eulerian analysis based on direct measurements [*Lukas*, 1986; *Steger et al.*, 1998] and numerical models [*Eden and Timmermann*, 2004; *Karnauskas et al.*, 2007] have shown that the Galapagos Islands represent a topographic barrier to the EUC that results in coastal upwelling west of the islands and causes the remainder of the current to split into two zonal eastward branches (flowing around the islands north and south of the equator) plus a southeastward branch [*Lukas*, 1986; *Karnauskas et al.*, 2007]. The two zonal eastward branches merge close to the equator just east of the islands [*Steger et al.*, 1998; *Karnauskas et al.*, 2007], whereas the southeastward branch of the EUC, formed between 92°W and 91°W converges with the pSSCC in the same longitude range [*Lukas*, 1986; *Karnauskas et al.*, 2007]. Our model domain extension prevents the exploration of this convergence. A similar merger, nevertheless, occurs farther east in the model within the computational domain, as we shall see. The above mentioned studies thus underscore the realism of the EUC behavior in our simulation.

[14] The subsurface counter currents, also known as the Tsuchiya Jets, are found a few degrees south of the EUC. In our simulations, the pSSCC is stronger than the sSSCC as observed in the eastern Tropical Pacific in previous studies [e.g., *Donohue et al.*, 2002]. It has been reported that their velocity cores rise and diverge away from the equator as they flow from west to east [*Furue et al.*, 2007, and references therein]. However, in the limited region that we simulate, the modeled pSSCC seems to maintain constant latitude (see section 3.2.1) as also observed by *Ishida et al.* [2005]. They hypothesized that this is due to that the driving mechanism of the pSSCC is different from that of the sSSCC. The pSSCC might sustain its zonal position owing to the westward and downward propagation of tropical instability waves [*Ishida et al.*, 2005] as was also argued by *Jochum and Malanotte-Rizzoli* [2004] for the Southern Equatorial Undercurrent (SEUC), an analogous current of the pSSCC in the Atlantic Ocean.

[15] Vertical cross sections of annual mean meridional velocity at ~12°S (+/-0.5°) for ROccam (Figure 3c) and RSoda (Figure 3d) simulations show the poleward Peru – Chile Undercurrent flowing along the shelf edge and the nearshore, equatorward Peru Coastal Current as described by *Gunther* [1936], *Silva and Neshyba* [1979], *Brockmann et al.* [1980], *Brink et al.* [1983], *Huyer* [1980], *Huyer et al.* [1991], and *Strub et al.* [1998], which form part of the Peru Current System. The PCUC, transporting mainly Equatorial Subsurface Water (ESSW) [*Silva et al.*, 2009], is widely recognized as a main source for the coastal upwelling off Peru and northern Chile [e.g., *Huyer et al.*, 1987]. Its core has been directly observed at 150 m depth over the slope offshore central Peru with velocities of about 10 cm s⁻¹ [e.g., *Huyer et al.*, 1991]. According to our simulations, at ~12°S (±0.5°), the core of the PCUC is located between 100 m and 150 m depth with maximum velocities around 12 cm s⁻¹ in the ROccam simulation. The core of the PCUC is located slightly deeper (120–170 m depth) with somewhat slower velocities of up to 10 cm s⁻¹ in the RSoda simulation.

[16] Both simulations capture Equatorial Current System and Peru Current System patterns consistent with the description given in previous studies. However, some differences in terms of depth, thickness, and intensity are observed between the two solutions: the maximum velocity core of the EUC is less intense and narrower in RSoda than in ROccam; the pSSCC is less intense but slightly wider in RSoda than in ROccam; the sSSCC is more intense, narrower and its lower limit is deeper in RSoda than ROccam; the PCUC is more intense in ROccam than in RSoda; and the PCC is wider and more intense in RSoda than in ROccam.

[17] Eulerian diagnostics allowed us to analyze the vertical structure of the horizontal velocity field, including all subsurface currents. The question we wish to address pertains to the origin and fate of water transported by some oceanic subsurface currents. Visually inferring water pathways from Eulerian velocity field can be difficult especially when the flow is fully three-dimensional and non stationary. Under these conditions, relying on streamlines for the mean horizontal velocity field can be misleading, e.g., at 100 m depth they indicate that the PCUC is directly fed by the EUC (Figure 2), and only Lagrangian trajectories will reveal the exact pathways.

3.2. Lagrangian Diagnostics

3.2.1. Pathways of the Subsurface Equatorial Currents and Their Contribution to the Peru-Chile Undercurrent

[18] In order to determine the pathways of the subsurface equatorial currents in the Eastern Tropical Pacific and how they connect with the Peru Current System we deployed numerical floats in each equatorial subsurface current (EUC, pSSCC, and sSSCC; between 86°–87°W, for details please refer to section 2). We first focused on identifying properly whether the floats remained flowing with their host current by considering only the floats which continued flowing eastward confined to the latitudinal band of their source current one month after being launched, and eliminated all other floats. Then, we tracked the float pathways forward in time, counting those passing through a cross-shore section at ~9°S, spanning from the coast of Peru to 82°W, encompassing almost exclusively the PCUC (Figure 4); floats crossing the

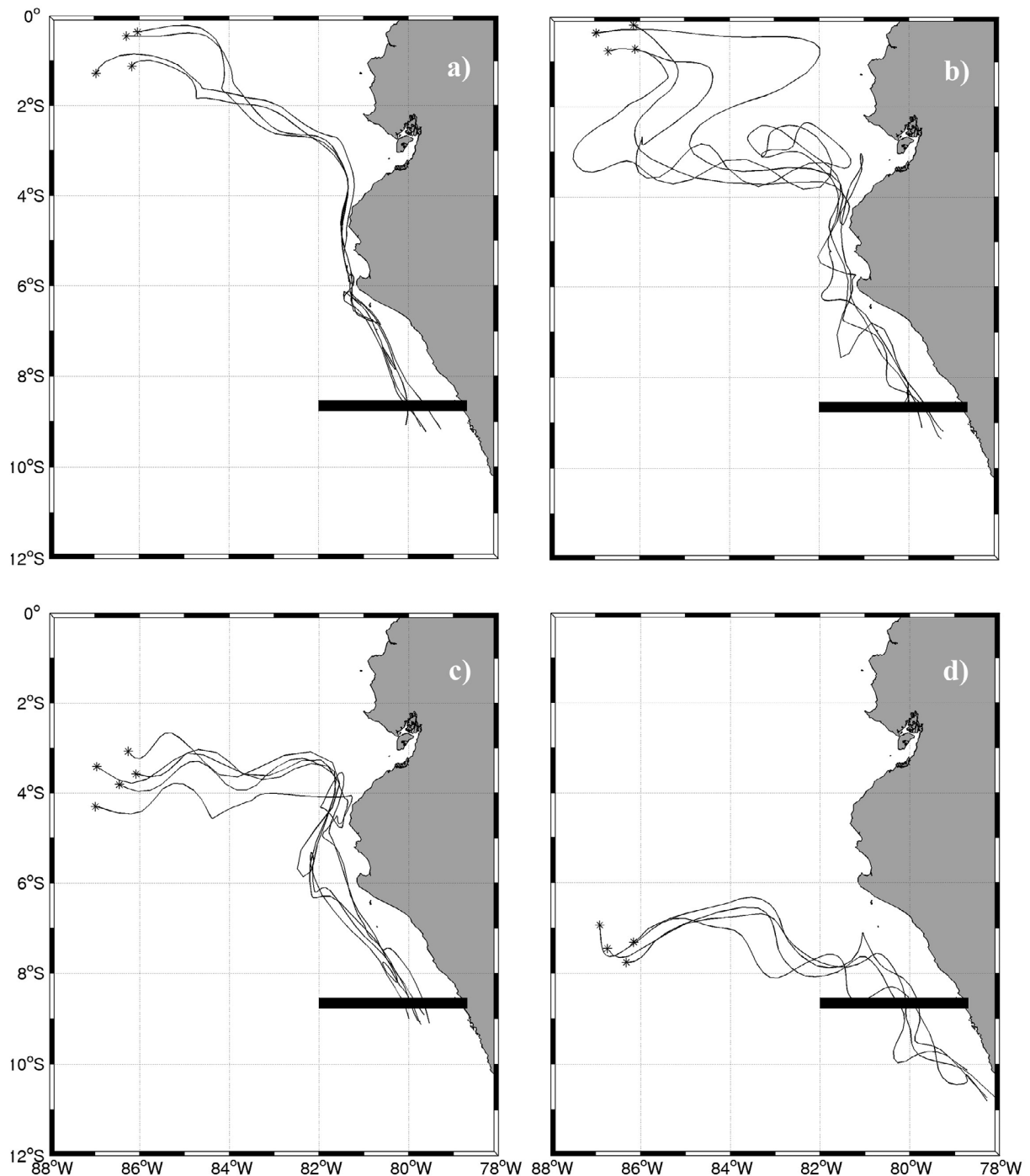


Figure 4. Examples of spaghetti diagrams showing typical routes of EUC, pSSCC, and sSSCC float trajectories that crossed the 9°S cross-shore section and thus became part of the PCUC: (a) EUC direct route, (b) EUC indirect route, (c) the pSSCC route, and (d) the sSSCC route. These diagrams include both simulations. Stars represent initial positions of released floats and the cross-shore black bar the PCUC-section that they crossed.

line within the top 10 m of the water column (an approximation of the mixed layer depth there) were separately counted.

[19] Out of the 36000 floats released in the EUC, we identified 22521 (28656) floats remaining within the current for at least one month and were thus considered EUC floats

(here as in the following ROccam solution appears first while RSoda numbers are put in parentheses). Only a small fraction of 4.5% (1.2%) reached the ~9°S cross-section offshore Peru, 4.3% (1.1%) below 10 m depth. Trajectories of these floats showed two routes toward the section. A direct route, where the floats flowed eastward along or southeastward of the

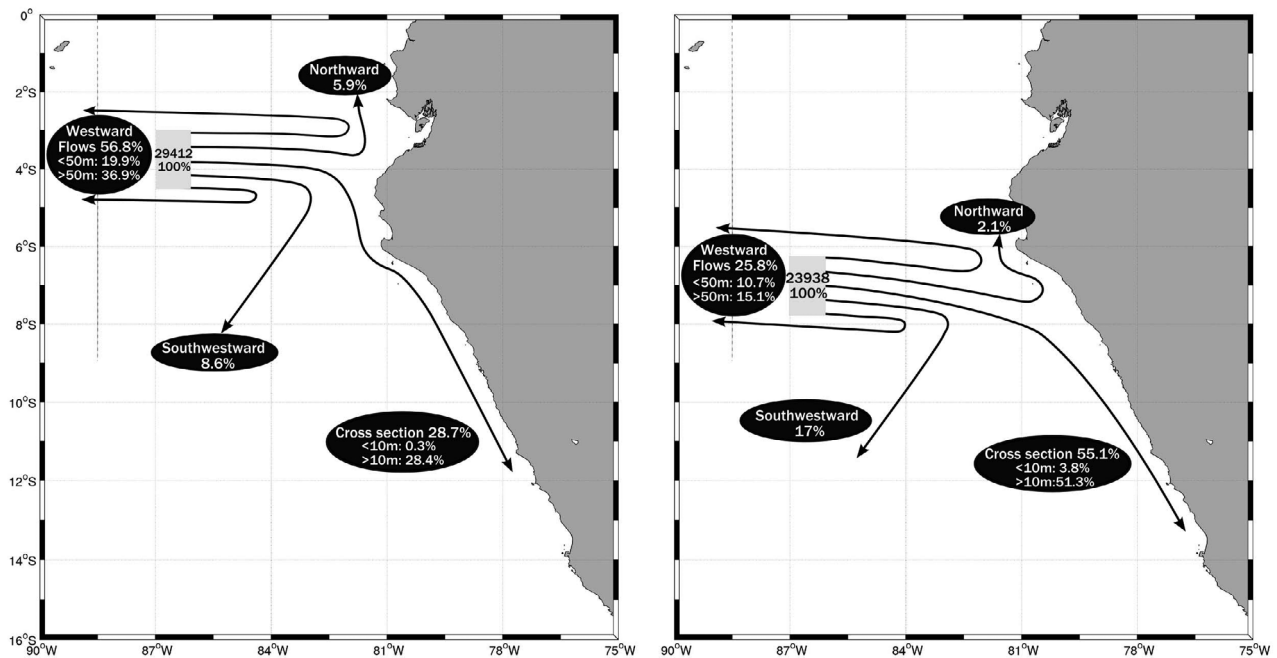


Figure 5. Scheme of the various paths of (left) the pSSCC and (right) the sSSCC floats according to ROccam; Out of the 36,000 floats released within the gray rectangular, 29,412 (pSSCC) and 23,938 (sSSCC) floats remained within the current for at least 1 month and then followed distinct routes indicated by black arrows and labels showing the percentage of floats occupied by each path, split up into various depth levels for westward flow (SEC) and poleward flow (PCUC). This scheme is also representative for the RSoda solution which only differs in the percentage of floats occupied by each path; pSSCC: 15.9% - northward, 32.6% - alongshore cross-section (0.3% above 10 m depth and, 32.3% below 10 m depth), 38.2% - westward flows (17.9% above 50 m depth and, 20.3% below 50 m depth), and 13.3% - turn southward; sSSCC: 2.9% - northward, 65.8% - alongshore cross-section (5.2% above 10 m depth and, 60.6% below 10 m depth), 19.1% - westward flows (7.9% above 50 m depth and, 11.2% below 50 m depth), and 12.2% - turn southward. The dashed line represents the westward boundary crossed by floats departing from their host currents and entering the SEC either north or south of the Equator.

equator reaching the coast of Peru at 4°S, then turned southward and continued along the coast (Figure 4a). Floats following the indirect route flowed several degrees of longitude along the equator eastward up to 83°W and then returned southwestward until joining the pSSCC toward the coast of Peru from where they continued flowing southward along the coast (Figure 4b). Without discriminating the followed route, it took them 4–24 months (14.25 months on average) to cross the 9°S section in both solutions.

[20] In the pSSCC, 29,412 (26,735) floats remained in their corresponding home current flowing eastward for at least one month; of these, 28.7% (32.6%) reached the cross-section at 9°S, i.e., formed part of the PCUC; 28.4% (32.3%) below 10 m depth. Out of the floats launched in the sSSCC, 23,938 (25,335) floats were identified as being trapped in the current, of which 55.1% (65.8%) crossed the section at 9°S; 51.3% (60.6%) below 10 m depth. In contrast to the EUC, only one pathway toward the 9°S section was identified for each of the SSCCs (Figures 4c and 4d). The pSSCC floats flowed zonally toward the coast then turned southward to continue flowing parallel to the coast, taking 2–24 months (13.5 months on average) to reach the section, in both solutions. The sSSCC floats flowed southeastward until arriving near to the coast, at ~8°S, and then flowed parallel to it. These floats needed 1–24 months (12.75 months on average) to cross the section.

In both simulations, the slowest floats were strongly affected by mesoscale activity before they reached the section.

[21] The remaining floats attached to the pSSCC and the sSSCC, namely the ones not crossing the nearshore section, followed a westward, a northward or a southwestward route (Figure 5); the percentages of floats corresponding to each route are summarized in Table 1. We first focused on identifying floats that became part of westward flows, by counting only those that crossed a meridional section located at 89°W (west of the launch site) between 4°N and 10°S, at any time after their release. We found that 56.8% (38.2%) of the pSSCC floats had trajectories that satisfied this definition; out of those, 19.9% (17.9%) above 50 m depth and 36.9% (20.3%) below 50 m depth (ROccam solution appears first;

Table 1. Percentage of Floats Associated With Each SSCC's Path^a

	Tsuchiya Jets	Westward	PCUC	Northward	Southwestward
pSSCC (3-day)		56.8	28.7	5.9	8.6
pSSCC (seasonal)		53.1	25.3	8.7	12.9
sSSCC (3-day)		25.8	55.1	2.1	17
sSSCC (seasonal)		2.7	63.9	0.3	33.1

^aStatistics are obtained from forward experiment with ROccam using 3-day and seasonal averaged velocity fields.

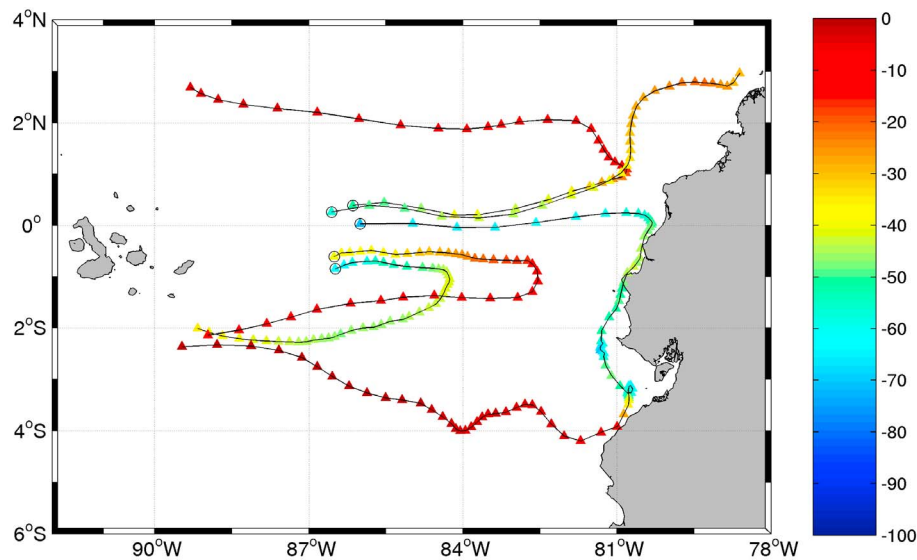


Figure 6. Spaghetti diagram illustrating the five typical trajectories of the EUC floats that did not cross the section $\sim 9^\circ\text{S}$. Circles mark the release positions, triangles the float positions in 3 days intervals and colors indicate float depth along the trajectories.

RSoda numbers are put in parentheses). Likewise, 25.8% (19.1%) of the sSSCC floats crossed the meridional section; 10.7% (7.9%) above 50 m depth and the rest below 50 m.

[22] The floats neither crossing the southern nor the western section described two different pathways for both SSCCs: a northward and southwestward route. The former first led zonally toward the coast then bended northward, roughly following the coast. The latter first went southeastward as far as 83°W and then turned southwestward until escaping the model domain. The northward pathway was followed by 5.9% (15.9%) of the pSSCC and 2.1% (2.9%) of the sSSCC floats while, the southwestward pathway was preferred by 8.6% (13.3%) of the pSSCC and 17% (12.2%) of the sSSCC floats.

[23] Some of the floats being part of the westward flows and/or the northward flow were subject to oceanic processes such as vertical advection, e.g., associated with coastal upwelling. This allowed them to reach the surface, where they were then trapped by surface currents, mainly the SEC. When examining trajectories, we also noticed that floats affected by coastal upwelling were strongly influenced by mesoscale activity before they flowed with the surface currents (not shown). This is consistent with *Penven et al.* [2005], who showed that a large number of eddies are generated from the upwelling front and propagate offshore [see *Penven et al.*, 2005, Figure 14], with larger and more intense eddies in the northern part of the Peruvian coastal region.

[24] East of 95°W the data availability is too limited to confirm or disprove the existence of the EUC and SSCCs routes toward the 9°S section taken by our numerical floats. The most recent work based on observational data for the eastern tropical Pacific was done at the end of the 1980s by *Lukas* [1986] who only reported the direct pathway of the EUC. However, recent OCGM-based studies on the dynamics of the Southern Tsuchiya jets (pSSCC and sSSCC) which were validated with western and central Pacific observations indicate direct and indirect EUC pathways in

agreement with our results. *Furue et al.* [2007] clearly showed the indirect route of the EUC. They found that the bottom part of the EUC bends southward then flowed westward and finally joined the top of the pSSCC. *Ishida et al.*'s [2005] results show that the pSSCC bifurcates between $100^\circ\text{--}90^\circ\text{W}$ into two branches. A northward branch which recirculates and feeds a westward flowing current on its equatorial flank, and a southward branch which connects to the PCUC. This is partly consistent with our circulation scheme (Figure 5) although the pSSCC bifurcation takes place farther west in *Ishida et al.*'s [2005] model. Moreover, in our solutions, the recirculation also occurs directly above the pSSCC indicating upwelling farther east and subsequent westward advection, and the equator-side recirculation is mainly sub-surface between 150–250 m depth. *Ishida et al.*'s [2005] sSSCC flows further south than in our solutions but also recirculates clockwise. Besides the main clockwise recirculation we also observe a weak counterclockwise recirculation.

[25] The results from ROccam and RSoda solutions are largely consistent regarding the pathways of the subsurface Equatorial Undercurrents. In particular both solutions show that only a small fraction of the EUC joins the PCUC in contrast with both SSCCs.

3.2.2. Fate of the EUC Floats

[26] The classical picture of the circulation in the Eastern Tropical Pacific shows that “although most of the EUC appears to flow all the way to the Peru coast in the thermocline, there is also substantial downstream loss of EUC water to the surface layer by upwelling” [*Kessler*, 2006]. However, the results of our simulations as well as those of *Blanke and Raynaud* [1997] reveal that only a very small fraction of the current reaches the coast and that the rest becomes part of equatorial upwelling, feeds westward currents such as the SEC, flows northward along the coast of central America, or contributes to coastal upwelling (Figures 6 and 7).

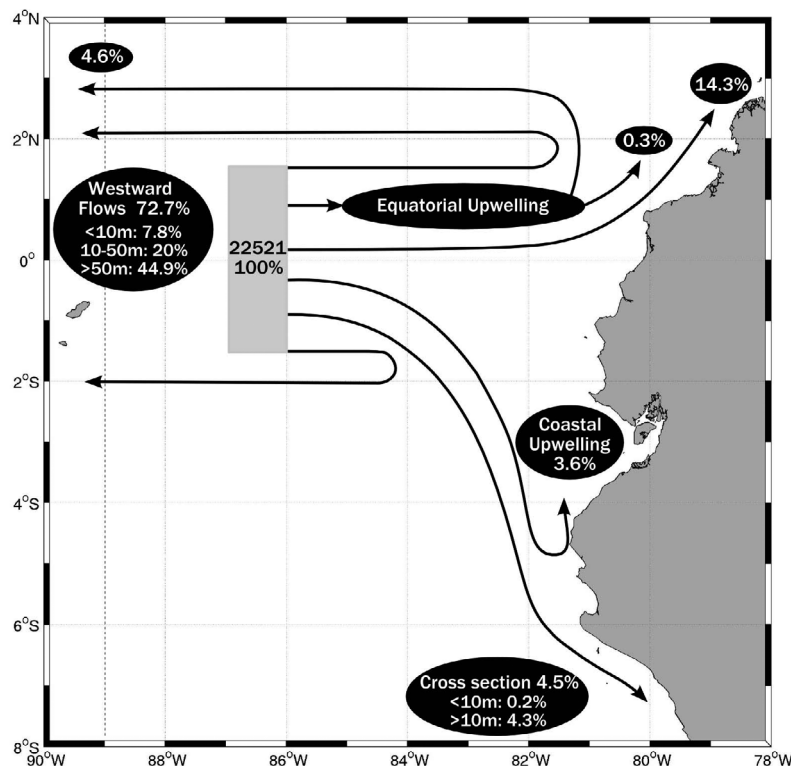


Figure 7. Scheme of the paths of the EUC floats according to ROccam, split up into various depth levels for westward flow (SEC) and poleward flow (PCUC). This scheme is also representative for the RSoda solution which only differs in the percentage of floats occupied by each path: the 28,656 floats identified as flowing with the EUC split up as follows: 7.8% - equatorial upwelling, 4.9% - coastal upwelling, 1.2% - alongshore cross-section (0.1% above 10 m depth and, 1.1% below 10m depth), 60.7% - westward (12.2% above 10 m depth, 28.9% between 10 m and 50 m depth and, 19.6% below 50 m depth), and 25.4% - northern route. The dashed line represents the westward boundary crossed by the floats leaving the EUC and entering the westward flows either north or south of the Equator.

[27] To quantify and distinguish these processes, we differentiated the EUC floats that did not cross the section at 9°S (i.e., that did not follow the routes to the PCUC) by introducing additional categories. First, we identified the floats that became part of the equatorial upwelling as those reaching 10 m depth within the first 105 days after their release. (This is to avoid counting floats that would upwell in the coastal upwelling. In fact all floats involved in the equatorial upwelling reached 10m depth within 72 days or less.) We found that equatorial upwelling heaved 4.9% (7.8%) of the floats toward the surface layers; this upwelling occurred mostly in a narrow equatorial band between 0.5°N – 2.5°S and 81° – 90°W . Most floats surfaced within the first 200 km offshore Ecuador; a smaller fraction escaped north to upwell offshore Colombia. Most of these upwelled floats later became part of the westward surface flow, namely the SEC.

[28] Next, we look for possible connections between the EUC and westward flows (whether surface – the SEC – or subsurface flows) by considering the float trajectories that neither crossed the 9°S section nor underwent equatorial upwelling as defined above. Out of those, the so-called *westward flowing floats* are defined as the ones which crossed a meridional section located at 89°W between 3°N and 10°S at any time, and at any depth, after remaining in the EUC for at least one month, regardless of their behavior in the Eastern

Tropical Pacific. This meridional section was chosen to be positioned well west of the launch area of the floats to ensure a significant westward transport. The latitudinal extent of the section is consistent with SEC locations reported in the literature [Wyrski, 1967; Lukas, 1986; Fuenzalida et al., 2008], and also coincides with the Eulerian outputs of our solutions. The meridional section was crossed by 7.8% (12.2%) of the floats above 10 m depth, 20% (28.9%) crossed between 10 and 50 m depth and the rest, 44.9% (19.6%), below 50 m depth. Most of the floats which entered the surface layer surfaced between the equator and 6°S , and thus were spread out farther than the floats that surfaced within the first 72 days; not any float left subsurface water between day 73 and 107. Recirculation mainly takes place in a narrow latitudinal band just south and north of the EUC but also above and below it, although to a lesser extent.

[29] The floats which fell in none of the three previous categories followed two different pathways: a northward and a southward route. The northern route first follows the equator toward the offshore region of Ecuador. From there some floats drift northward, roughly along the coast, and enter the Panama Bight, whereas others turn west before heading north at about the longitude of the Galapagos Islands and subsequently escape the study region. The northern route is taken by 14.3% (25.4%) of the EUC floats. The southern

Table 2. Feeding Sources of the PCUC Obtained From the Backward Experiment by ROccam and RSoda^a

Solutions	EUC	pSSCC	sSSCC	Southern Domain	Alongshore
ROccam (%)	2.3	9.4	13.8	39.5	35
RSoda (%)	1.1	11.1	20.8	31.7	35.3
ROccam (Sv (%PCUC))	0.09 (2,3)	0.46 (11,8)	0.85 (21.9)	1.44 (36.9)	1.06 (27.1)
RSoda (Sv (%PCUC))	0.06 (1,4)	0.71 (14,5)	1.23 (24.9)	1.85 (37.5)	1.07 (21.7)

^aThe 3-day average of ROccam and RSoda are used here. Shown are the percentage of floats and a quasi volume transport, in Sv and its percentage contribution to the PCUC, associated with each source for both solutions.

route is followed by fewer floats, 3.6% (4.9%). The latter floats emerge in the northern part of the Peruvian coastal region, in the intense upwelling plume known as the Paita upwelling region ($\sim 5^{\circ}\text{S}$) [Maeda and Kishimoto, 1970]. Figure 7 illustrates the results obtained with our criterion and shows all the possible pathways and contributions for both, ROccam and RSoda, solutions.

[30] ROccam and RSoda pathways for the EUC water are very similar and their respective percentages of occurrence are not inconsistent. Therefore, the differences between the two Eulerian solutions do not lead to qualitatively different Lagrangian results, which is an important sign of robustness. In particular, both solutions suggest that most part of the EUC water contributes to the SEC or deeper flows below it, and only a little continues flowing southward along the Peruvian coast.

3.2.3. Feeding Sources of the PCUC

[31] In order to determine the origin of the PCUC water, we released numerical floats between 30 and 400 m depth on a cross-shore section encompassing the PCUC at 12°S ($\pm 0.5^{\circ}$) (Figure 2). The floats were tracked backward in time for 3 climatological years and, as in the previous section, we applied selection tests to identify only the floats truly flowing in the PCUC (hereafter referred to PCUC floats). First, we selected all the floats being still within the PCUC north of the 12°S cross-section one month after being released and traced backward. Out of the 3809 floats released in each of the two simulations, 3321 (2369) floats remained below 30 m depth, in backward mode, within the PCUC. A further selection consisted in only keeping the floats whose trajectory crossed the 88°W section with no requirement on the travel duration (other than the 3 year time period over which the backward experiment is carried out). We partitioned the 88°W longitude into different subsets according to the latitudinal distribution of floats crossing this section. Three of the four subsets match the latitudinal ranges of the EUC (1.5°N – 1.5°S), the pSSCC (2°S – 4.7°S), and the sSSCC (5.8°S – 8.2°S). The fourth subset (south of 8.5°S) corresponds to floats from western non-equatorial origin. Floats which did not reach 88°W during the three years duration of the backward experiment are discussed below.

[32] Backward results highlighting the distinct sources of the PCUC obtained using 3-day average velocity fields from ROccam and RSoda are summarized in Table 2. Out of the floats released at the 12°S offshore cross-section and which qualified to be PCUC floats according to their residence time in the current, 2.3% (1.1%) originated in the EUC, 9.4% (11.1%) in the pSSCC and 13.8% (20.8%) in the sSSCC. All these floats crossed the western section from west to east 1–3 years before reaching the 12°S offshore cross-section, and were located at depths between 40–300 m (Figure 8), i.e., well within the vertical extent of the equatorial

undercurrents, without applying any prior restriction. The percentage of PCUC-floats not stemming from equatorial western sources but crossing the 88°W longitude south of 8.5°S were 39.5% (31.7%). Their trajectories revealed the presence of a weak eastward flow occurring at more than 100 m depth in the southern part of the domain.

[33] The number of floats which did not cross the western section within 3 years accounted for 35% (35.3%). Their pathways depicted an alongshore recirculation associated with flow below the PCUC (Figure 8). These PCUC floats indicate the existence of water injection into the PCUC from below. A northward flow, with alongshore velocity of around 2 cm s^{-1} , could be identified in the model Eulerian fields just underneath the PCUC extending down to 1500 m which feeds this injection. As revealed from the float trajectories, water slowly upwells from abyssal depths into the PCUC while it is being carried equatorward by this flow as far north as 3°S (once the floats are inside the PCUC they start flowing poleward). This recirculation was so far not considered in the general scheme of the contributions for the PCUC [e.g., Strub *et al.*, 1998].

[34] Density and longitude at 12°S (i.e., position in the PCUC relative to the coast) associated with each of the five water sources of the PCUC are represented in Figure 8 (inlay). EUC and SSCCs water characteristics mostly overlap and this is consistent with the fact that mixing between these equatorial currents should be vigorous (e.g., see Jochum and Malanotte-Rizzoli [2004] for the Atlantic Ocean). The other two sources can be better identified. The heaviest (1025.84 kg m^{-3}) water stems from the southern domain and flows along the western flank of the current. The second heaviest (1025.68 kg m^{-3}) water corresponds to the upwelling from below the PCUC and is mainly present on its eastern flank. The core of the current is made up of equatorial sources out of which EUC water is the lightest (1025.44 kg m^{-3}), closely followed by pSSCC (1025.46 kg m^{-3}), and then sSSCC water (1025.65 kg m^{-3}).

[35] It is sometimes convenient to consider the volume transport contribution associated with various feeding sources of a current [Goodman *et al.*, 2005]. By assigning each float an area according to the distribution of floats within the release region (see Figure 3) and multiplying it by the particle's velocity, we were able to compute such volume transports for each of the PCUC water sources (see Table 2). Results are quite similar for ROccam and RSoda. The upwelling from below (alongshore recirculation) accounted for about 1 Sv, 1.5 Sv stemmed from the southern domain, 1.5 Sv came from the SSCCs, and the EUC contributed less than 0.1 Sv (note that the PCUC transports are respectively 3.9 Sv and 4.9 Sv in the ROccam and RSoda solution which is in the order of observational data, e.g., 4 Sv [Wyrski, 1963]).

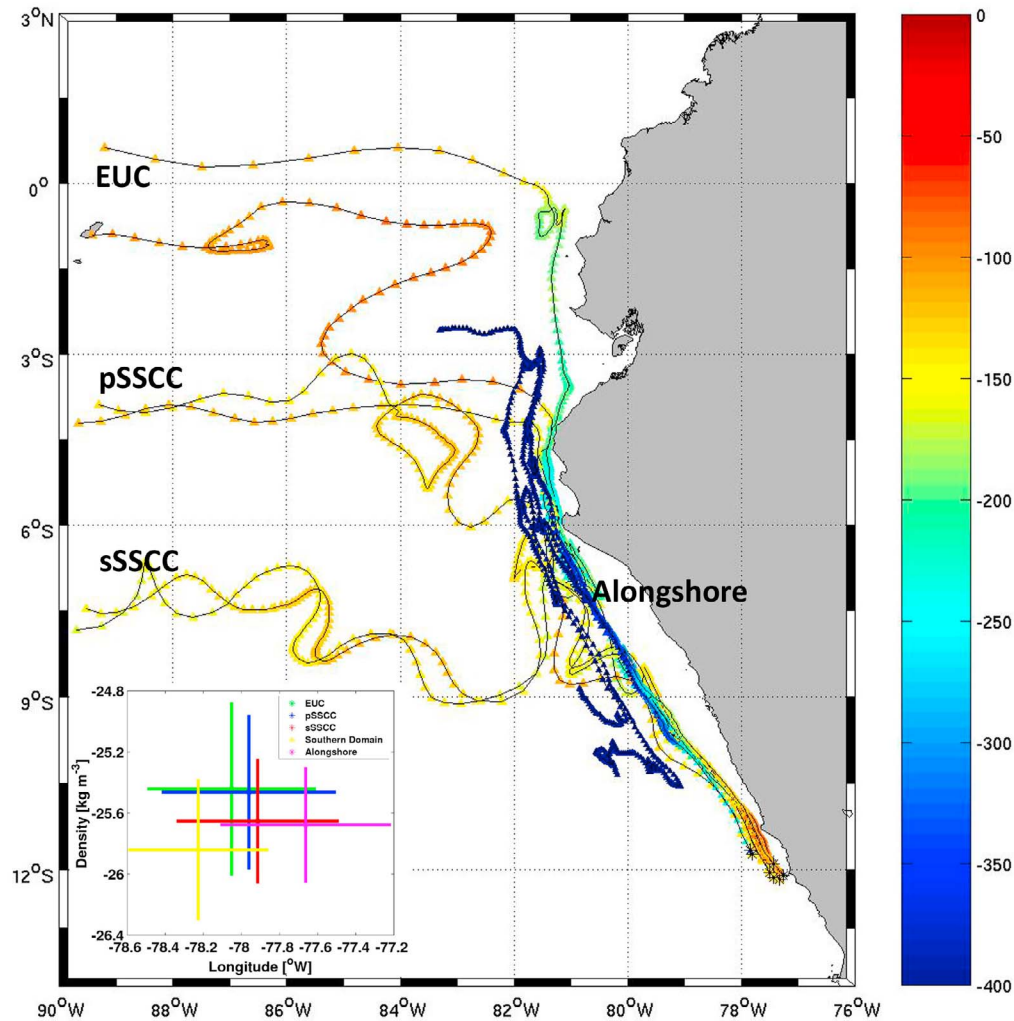


Figure 8. Typical pathways of the feeding sources of the PCUC revealed by the backward experiment. Stars near the coast (around 12°S) indicate the initial position of the floats and colors along the pathways their depth according to the color bar on the right-hand side of the figure. The PCUC is fed to about 60% by the main subsurface equatorial flows (EUC, pSSCC, sSSCC) and by the alongshore recirculation. A diagram presenting density distribution along the PCUC section of the backward experiment, 11.5°S–12.5°S ($\pm 0.5^\circ$), identifying the contribution of each source water, is inserted in the lower-left corner. Each source water is assigned a different color (see legend). Mean density (σ_t) and mean longitude together with standard deviations are plotted by vertical and horizontal bars where the center of the cross presents the mean and the bars two standard deviations.

[36] The backward experiment applied to both solutions, ROccam and RSoda, shows that the main source to the PCUC, between three subsurface equatorial currents, is the sSSCC followed by the pSSCC and then the EUC, the latter being less important; this is in agreement with the forward experiment results. Most remarkable, this experiment suggests that there are two other non-equatorial sources to the PCUC: one associated with flows below the PCUC (called here alongshore recirculation) and another associated with flows occurring in the southern part of the domain (south of 8.5°S).

3.2.4. Role of the Eddies

[37] In order to understand a possible effect of the mesoscale variability on the different pathways previously described, we repeated the Lagrangian forward experiment

(section 3.2.1) using seasonal averaged (over 5 years) instead of 3-day averaged ROccam velocity fields. Results are presented in Table 1, only for the SSCCs since there is almost no difference between the two experiments for the EUC (e.g., only 0.7% difference for the EUC/PCUC connection). The most important change concerns the sSSCC/westward connection when going from seasonal to 3-day averages. The mesoscale variability strongly reinforces the sSSCC contribution to the westward flows to the detriment of its southwestward contribution. It also alters its connection with the PCUC (from 63.9% to 55.1%). The pSSCC case is different: its contribution to the PCUC is clearly enhanced in the 3-day average experiment.

[38] To further illustrate the role of the eddies, and the difference between the seasonal and the 3-day average

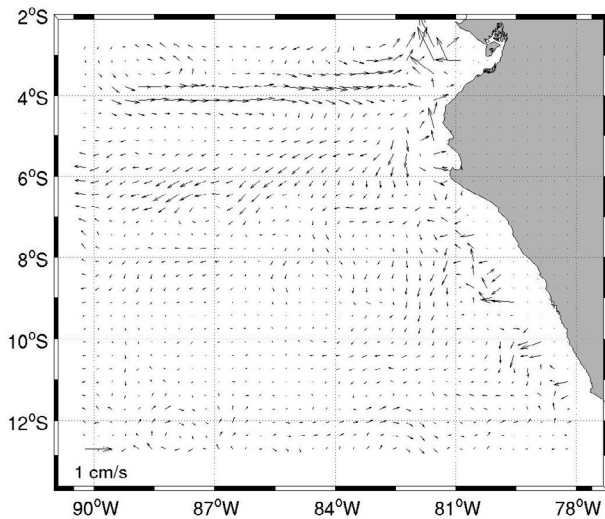


Figure 9. Eddy-induced velocity computed for the density layer [25.2; 25.8], using 4 years of the ROccam solution.

experiments, we estimated an eddy-induced velocity (EIV) with the ROccam outputs. The eddy-induced velocity [McWilliams and Danabasoglu, 2002], u^* , is defined as

$$u^* = \frac{\overline{uh}}{h} - \bar{u},$$

where u is the horizontal velocity, and h is the density layer thickness.

[39] The EIV has been computed for the density layer [25.2; 25.8]. This layer has been chosen after examining (not shown) the density range for the particles flowing with the equatorial currents into the PCUC. This layer does not outcrop at any time. The particle densities stay within this range all along their pathways to the east, except once in the near-shore region where they can be subject to diabatic processes associated with the upwelling.

[40] The EIV has been computed using 4 years of 3-day outputs and is presented in Figure 9. Coherent patterns emerge on this map, especially an eastward advection along the pSSCC path, with values around 1 cm s^{-1} or less (which is of the order of one tenth of the mean velocity). Southwestward advection ($\sim 0.5 \text{ cm s}^{-1}$) is also noticeable in the vicinity of the sSSCC path.

[41] These two features are not inconsistent with the most significant changes resulting from the presence of eddies (Table 1), i.e., the increase (reduction) of the pSSCC (sSSCC) water that feeds the PCUC could be related to the favorable (unfavorable) eddy advection. Most importantly, EIV velocities in the vicinity of the sSSCC tend to advect water away from the Peruvian upwelling. Large nearshore EIV values oriented to some extent cross-shore could also lead to subtle modifications in the final connecting stage between the PCUC and SSCCs.

[42] Overall, these results indicate that the mesoscale exerts a significant modulation role on the pathways and the connections between the PCUC and its equatorial sources. Eddy advection which we studied in detail is responsible for part of that modulation but eddy mixing (in particular isopycnal

mixing) could also well be important when trying to understand the eddy role.

4. Conclusions

[43] In this study, we used 3-day averaged velocity fields from eddy-resolving regional solutions (ROMS), with two different boundary conditions in order to understand the transport relationship between the Equatorial Current System and the Peru Current System. By means of Lagrangian tracking, we released a large number of particles in each equatorial subsurface current (EUC, pSSCC and sSSCC) to study and describe their fate in the Eastern Tropical Pacific and their contribution to the Peru-Chile Undercurrent.

[44] Although a detailed study about the sensitivity of regional simulations to their boundary conditions is beyond the scope of this paper, we analyzed annual mean velocity fields for two simulations. Both resembled well the known regional dynamics but they differed slightly in the currents' vertical structure. Nevertheless, the Lagrangian diagnostics revealed that both simulations presented similar pathways, similar connections and very small differences in their respective contribution percentages. This gives us confidence in the robustness of our results vis-à-vis the biases and uncertainty present in our model circulations.

[45] Regardless of the solution, the EUC contributions to coastal upwelling of northern Peru and feeding the PCUC are small. This remains true even when the fraction of the water which upwells in the Equatorial upwelling is not counted, a viewpoint adopted from Cravatte *et al.* [2007] (9.1% - ROccam, 7.6% - RSoda). Instead most of that water (about 70%) recirculates within westward flows, i.e., the SEC and deeper flows below it, while another significant fraction (approximately 24%) continues to flow eastward till the coast from where it turns northward along the coast or contributes to the North Equatorial Current.

[46] Lagrangian tracking applied to the pSSCC (sSSCC) showed that $\sim 25\%$ ($\sim 50\%$) of the water carried by this current reached the coast and fed the PCUC. The SSCCs/PCUC connections were affected by mesoscale activity along their paths, especially in the case of the sSSCC.

[47] The PCUC, which owes its existence to alongshore winds favorable to upwelling [McCreary, 1981], is fed directly to about 30% by the three subsurface equatorial sources (EUC, pSSCC, sSSCC). The remaining stems from upwelling from below the PCUC (and an associated along-shore equatorward circulation - 35%) and weak diffuse currents present in the southern part of the domain (south of $\sim 9^\circ\text{S}$ - 35%).

[48] An important and striking result is that among the different PCUC equatorial sources, the EUC is by far the weakest. Different previous studies, based on hydrographic data [e.g., Wyrтки, 1967; Lukas, 1986] or coarse resolution model [e.g., Cravatte *et al.*, 2007], have hypothesized or reported a strong connection between the EUC and the PCUC, describing the PCUC as largely fed by the EUC. The EUC and the SSCCs carry water masses (present in the PCUC) with similar T/S characteristics (this is also the case in our solutions - not shown). Analysis mainly based on hydrography, with a somewhat limited amount of data, can lead to that conclusion, while omitting the role played by the SSCCs. Other studies have more recently described a very

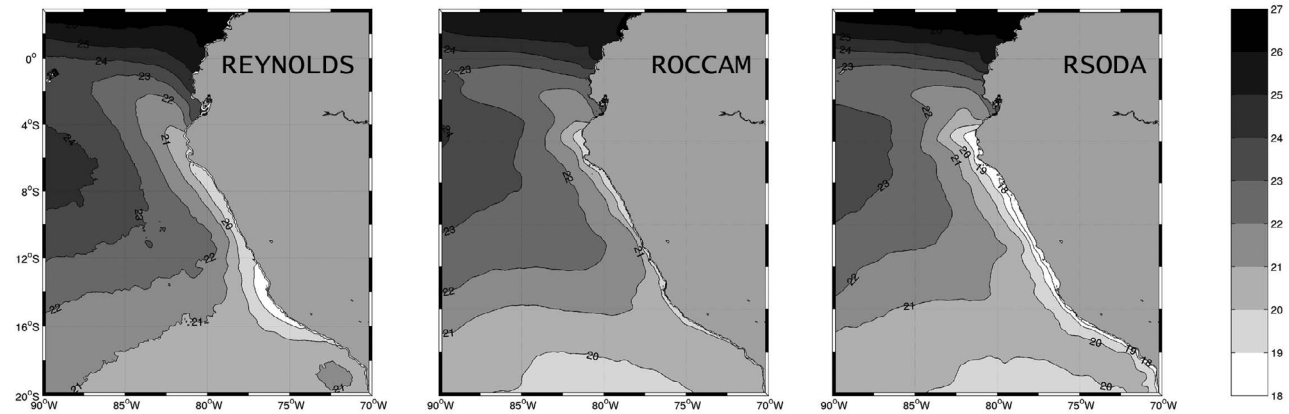


Figure A1. Annual mean sea surface temperature ($^{\circ}\text{C}$) of the entire model domain for (left) the Reynolds climatology, (middle) the ROccam model, and (right) the RSoda model. Sea surface temperature is shaded in gray tones (to relate gray tones to temperature refer to the gray tone bar on the right-hand side), and line contoured (black solid lines) with intervals of 1°C .

possible connection between the SSCCs and the PCUC [e.g., *Johnson and Moore, 1997; Donohue et al., 2002*], but to our knowledge our study is the first one using a regional eddy-resolving model to quantify these connections and clearly shows that the main PCUC equatorial sources are the SSCCs and not the EUC.

[49] All these results show a clear connection between the PCUC and large-scale equatorial currents. Hence variations

of the latter on any time scale (e.g., interannual related to ENSO) need to be investigated, since they presumably affect the PCUC variability and in turn the coastal upwelling that uplifts PCUC water. Studying the way the connections are disrupted or strengthened on interannual time scales (mostly in relation with the large-scale variability of the Equatorial system) is of primary importance. On time scales perhaps a bit longer the Peruvian system may also influence, through

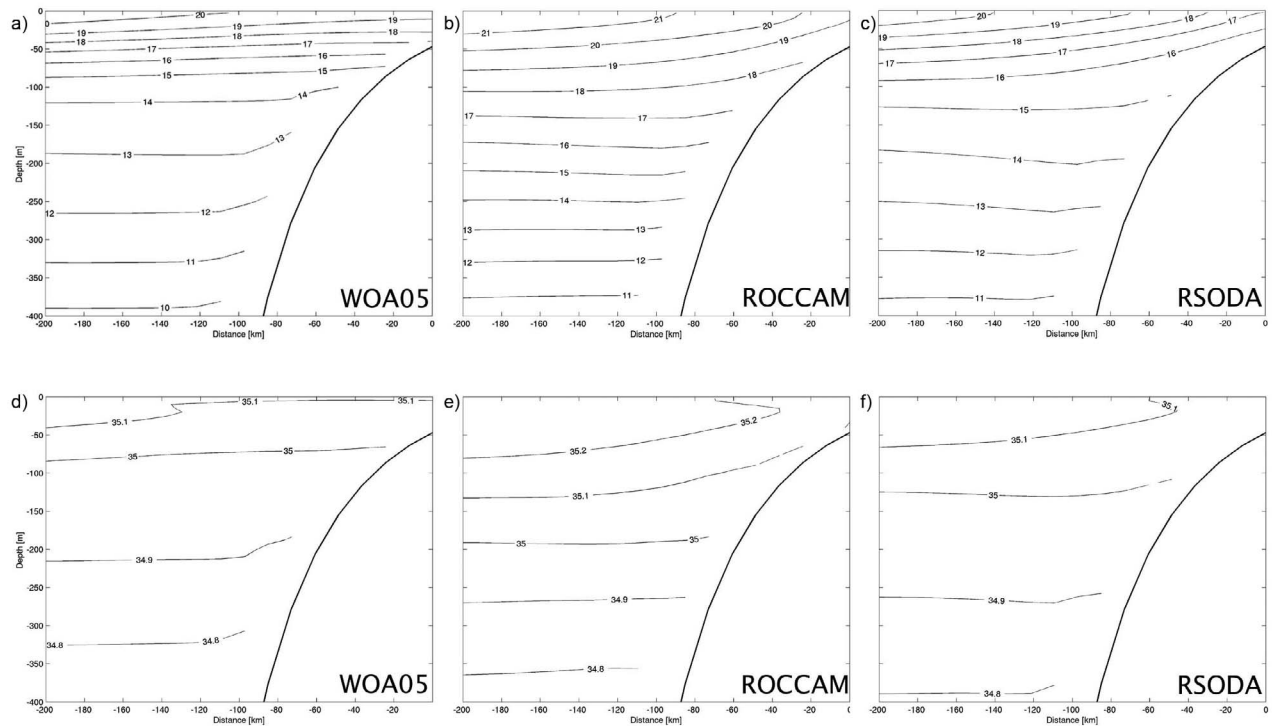


Figure A2. Vertical cross sections of (a–c) annual mean temperature and (d–f) salinity averaged from 7°S to 13°S for the central Peruvian upwelling region based on World Ocean Atlas 2005 climatology (Figures A2a and A2d), ROccam model (Figures A2b and A2e), and RSoda model (Figures A2c and A2f). Temperature (salinity) is contoured with black solid lines with intervals of 1°C (0.1 PSU).

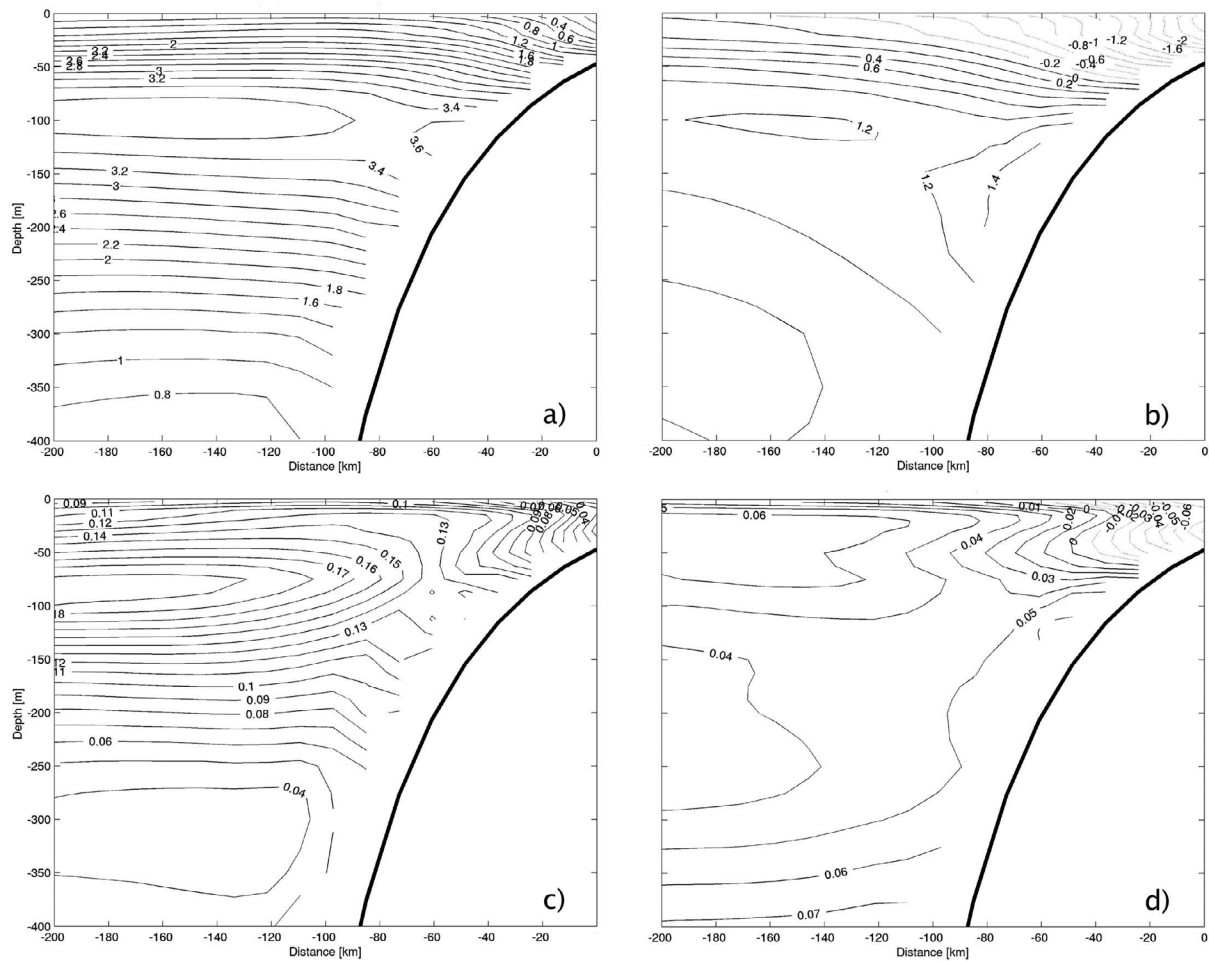


Figure A3. (a and b) Temperature and (c and d) salinity biases between the model solutions and WOA05 for the section shown in Figure 2. ROccam minus WOA05 is shown in Figures A3a and A3c and RSoda minus WOA05 in Figures A3b and A3d. Temperature (salinity) is contoured with black solid lines with intervals of 0.2°C (0.01 PSU).

upwelling, the Equatorial current system and in particular the structure of the SSCCs. This type of feedback has been established in idealized models [e.g., *McCreary et al.*, 2002] but its relevance to the real ocean is still debated. By definition the offline nesting strategy employed to obtain the ROccam and RSoda does not allow us to consider this subtle retroaction, because large scale equatorial currents – coming from the SODA or OCCAM models – cannot feel the effects resulting from better reproduced upwelling in the PCS in eddy-resolving regional models [*Capet et al.*, 2008]. Conversely, it is plausible that the regional solutions we analyze by Lagrangian means have a Peruvian system that is not exactly in equilibrium with their (externally prescribed) Equatorial system. Again, the robustness of our results vis-à-vis changes of the lateral boundary conditions suggests that this issue does not invalidate our study: moderate changes in the equatorial current system do not dramatically affect the fate and origin of the water carried by the major Eastern Tropical Pacific currents we have considered. However, we believe it provides an additional motivation for studying Equatorial/Peru systems connections in a basin-

scale configuration that would adequately resolve mesoscale activity whose role is important as we demonstrated.

Appendix A: Model Validation Summary

[50] The numerical quasi-equilibrium solutions we analyzed were obtained with Regional Ocean Model Systems (ROMS) using the model configuration developed by *Penven et al.* [2003, 2005] (for details see section 2), here referred to as ROccam. The sensitivity to these boundary conditions is assessed by performing an additional simulation based on the V. Echevin et al. (personal communication, 2009) configuration, here called RSoda, that is identical to ROccam in every aspect but the open boundary conditions, derived from a climatology of the SODA global ocean reanalysis at $1/2^{\circ}$ resolution [*Carton and Giese*, 2008] (for details see section 2). The ROccam and RSoda solutions were validated by *Penven et al.* [2005] and V. Echevin et al. (personal communication, 2009), respectively. Here we briefly summarize some of their validation results and present additionally an annual mean SST, and an annual mean vertical

temperature/salinity section model versus observations comparison, as well.

[51] The evaluation of the ROccam and RSoda model skills was done by a general comparison of the model averaged circulation, the seasonal cycle, and the mean baroclinic structure with annual or seasonal climatologies and with what has been published in the literature.

[52] The major known currents in the Peru Current system were rendered quite accurately. The models reproduced the coastal dynamics of the Peru Coastal Current which flows equatorward in a band of 100 km from the shore, the location and vertical extension, with current speeds in the range of observations, of the Peru Chile Under Current which follows the shelf break toward the pole, and the Peru Chile Counter Current which runs toward the south.

[53] Mean eddy kinetic energy (EKE) was computed using the geostrophy from sea surface height for both the model simulations and satellite-borne altimeter observations (AVISO). Model and altimeter EKE followed the same pattern with high values in the upwelling front and close to the Equator, and lower values offshore. For the central Peru Current system, ROccam EKE was 10–30% lower than in observations, but significantly lower near the Equator and in the southern part of the domain. Similar results were obtained for the RSoda simulation. Even if the levels of EKE in both simulations were too low, we are confident, at least qualitatively, that the model's output is suitable to study the meso-scale dynamics in the Peru current system with a relatively realistic level of energy.

[54] In general, ROccam's SST underestimates Pathfinder surface temperatures (mean 1985–1997 satellite sea surface temperature) by 0.5°C. When comparing the model SSTs with Reynolds surface temperatures (a climatology derived from monthly Optimum Interpolation SST analyses with an adjusted base period of 1971–2000) the difference increased to an underestimation of 0.7°C for ROccam and 0.8°C for RSoda. Nevertheless, the main oceanographic features of the region, the equatorial temperature front, coastal upwelling along the Peruvian coast, and the intrusion of colder waters from the south by means of the Humboldt Current, are realistically reproduced in both simulations (Figure A1) despite minor systematic differences in SST. This gives us confidence that both solutions are able to reproduce surface oceanic patterns with certain realism.

[55] As for the mean vertical baroclinic structure, the most striking feature is the very sharp thermocline and to a lesser extent the halocline (Figure A2). Mean temperature (salinity) in the section shown in Figure A2 was 1.5°C (0.08 PSU) and 1.2°C (0.04 PSU) warmer (saltier) than in WOA05 in ROccam and RSoda, respectively. Significant differences (2–3°C), however, between WOA05 and ROccam arose in the thermocline (Figure A3).

[56] In summary, we conclude that the model simulations reproduce well the known average circulation, the seasonal cycle, and the mean baroclinic structure in the Eastern Tropical Pacific and hence the quasi-equilibrium climatological solutions are apt to unravel regional aspects of the ocean dynamics.

[57] **Acknowledgments.** We are deeply indebted to P. Peven for the work and the help he devoted to initiate regional modeling studies at the Instituto del Mar del Peru (IMARPE) where I. Montes and F. Colas started this work. We also thank him for providing us with the ROccam solution.

We also thank F. Bryan, R. Furue, and an anonymous reviewer for their suggestions and comments to improve this manuscript. The first author was funded by the Deutscher Akademischer Austausch Dienst (DAAD) scholarship and by the Chilean National Research Council through the FONDAP-COPAS Center. F. Colas was funded by IMARPE and the IRD (Institut de Recherche pour le Développement) during his stay at IMARPE at the initial stage of this work.

References

- Blanke, B., and S. Raynaud (1997), Kinematics of the Pacific Equatorial Undercurrent: An Eulerian and Lagrangian approach from GCM results, *J. Phys. Oceanogr.*, **27**, 1038–1053, doi:10.1175/1520-0485(1997)027<1038:KOTPEU>2.0.CO;2.
- Blanke, B., M. Arhan, A. Lazar, and G. Prévost (2002), A Lagrangian numerical investigation of the origins and fates of the salinity maximum water in the *Atlantic*, *J. Geophys. Res.*, **107**(C10), 3163, doi:10.1029/2002JC001318.
- Brink, K. H., D. Halpern, A. Huyer, and R. L. Smith (1983), The physical environment of the Peruvian upwelling system, *Prog. Oceanogr.*, **12**, 285–305, doi:10.1016/0079-6611(83)90011-3.
- Brockmann, C., E. Fahrback, A. Huyer, and R. L. Smith (1980), The poleward undercurrent along the Peru coast: 5 to 15°S, *Deep Sea Res. Part A*, **27**, 847–856, doi:10.1016/0198-0149(80)90048-5.
- Capet, X. J., P. Marchesiello, and J. C. McWilliams (2004), Upwelling response to coastal wind profiles, *Geophys. Res. Lett.*, **31**, L13311, doi:10.1029/2004GL020123.
- Capet, X., F. Colas, P. Penven, P. Marchesiello, and J. McWilliams (2008), Eddies in eastern boundary subtropical upwelling systems, in *Ocean Modeling in an Eddy Regime*, *Geophys. Monogr. Ser.*, vol. 177, edited by M. W. Hecht and H. Hasumi, pp. 131–147, AGU, Washington, D. C.
- Carr, S., X. Capet, J. McWilliams, J. T. Pennington, and F. P. Chavez (2008), The influence of diel vertical migration on zooplankton transport and recruitment in an upwelling region: Estimates from a coupled behavioral-physical model, *Fish. Oceanogr.*, **17**, 1–15.
- Carton, J. A., and B. S. Giese (2008), A reanalysis of ocean climate using Simple Ocean Data Assimilation (SODA), *Mon. Weather Rev.*, **136**, 2999–3017, doi:10.1175/2007MWR1978.1.
- Chavez, F. P., A. Bertrand, R. Guevara-Carrasco, P. Soler, and J. Csirke (2008), The northern Humboldt Current System: Brief history, present status and a view towards the future, *Prog. Oceanogr.*, **79**, 95–105, doi:10.1016/j.pocan.2008.10.012.
- Colas, F., X. Capet, J. C. McWilliams, and A. Shchepkin (2008), 1997–1998 El Niño off Peru: A numerical study, *Prog. Oceanogr.*, **79**, 138–155, doi:10.1016/j.pocan.2008.10.015.
- Cravatte, S., G. Madec, T. Izumo, C. Menkes, and A. Bozec (2007), Progress in the 3-D circulation of the eastern equatorial Pacific in a climate ocean model, *Ocean Modell.*, **17**, 28–48, doi:10.1016/j.ocemod.2006.11.003.
- Cromwell, T., R. B. Montgomery, and E. D. Stroup (1954), Equatorial Undercurrent in Pacific Ocean revealed by new methods, *Science*, **119**, 648–649, doi:10.1126/science.119.3097.648.
- Da Silva, A. M., C. C. Young, and S. Levitus (1994), *Atlas of Surface Marine Data 1994*, vol. 1, *Algorithms and Procedures*, NOAA Atlas NESDIS, vol. 6, 83 pp., NOAA, Silver Spring, Md.
- Donohue, K. A., E. Firing, G. D. Rowe, A. Ishida, and H. Mitsudera (2002), Equatorial Pacific subsurface countercurrents: A model-data comparison in stream coordinates, *J. Phys. Oceanogr.*, **32**, 1252–1264, doi:10.1175/1520-0485(2002)032<1252:EPSCAM>2.0.CO;2.
- Eden, C., and A. Timmermann (2004), The influence of the Galápagos Islands on tropical temperatures, currents and the generation of tropical instability waves, *Geophys. Res. Lett.*, **31**, L15308, doi:10.1029/2004GL020060.
- Fiedler, P. C., and L. D. Talley (2006), Hydrography of the eastern tropical Pacific: A review, *Prog. Oceanogr.*, **69**(2–4), 143–180, doi:10.1016/j.pocan.2006.03.008.
- Fuenzalida, R., W. Schneider, J. Garcés-Vargas, and L. Bravo (2008), Satellite altimetry data reveal jet-like dynamics of the Humboldt Current, *J. Geophys. Res.*, **113**, C07043, doi:10.1029/2007JC004684.
- Furue, R., J. P. McCreary, Z. Yu, and D. Wang (2007), The dynamics of the southern Tsuchiya Jet, *J. Phys. Oceanogr.*, **37**, 531–553, doi:10.1175/JPO3024.1.
- Goodman, P. J., W. Hazeleger, P. de Vries, and M. Cane (2005), Pathways into the Pacific Equatorial Undercurrent: A trajectory analysis, *J. Phys. Oceanogr.*, **35**, 2134–2151, doi:10.1175/JPO2825.1.
- Gunther, E. R. (1936), A report on oceanographic investigations in the Peru Coastal Current, *Discovery Rep.* **13**, pp. 107–276, Cambridge Univ. Press, Cambridge, U. K.

- Huyer, A. (1980), The offshore structure and subsurface expression of sea level variations off Peru, 1976–1977, *J. Phys. Oceanogr.*, *10*, 1755–1768, doi:10.1175/1520-0485(1980)010<1755:TOSASE>2.0.CO;2.
- Huyer, A., R. L. Smith, and T. Paluszkiwicz (1987), Coastal upwelling off Peru during normal and El Niño times, *J. Geophys. Res.*, *92*, 14,297–14,307, doi:10.1029/JC092iC13p14297.
- Huyer, A., M. Knoll, T. Paluszkiwicz, and R. L. Smith (1991), The Peru Undercurrent: A study of variability, *Deep Sea Res. Part A*, *38*, S247–S271.
- Ishida, A., H. Mitsudera, Y. Kashino, and T. Kadokura (2005), Equatorial Pacific subsurface countercurrents in a high-resolution global ocean circulation model, *J. Geophys. Res.*, *110*, C07014, doi:10.1029/2003JC002210.
- Jochum, M., and P. Malanotte-Rizzoli (2004), A new theory for the generation of the equatorial subsurface countercurrents, *J. Phys. Oceanogr.*, *34*, 755–771, doi:10.1175/1520-0485(2004)034<0755:ANTFTG>2.0.CO;2.
- Johnson, G. C., and M. J. McPhaden (1999), Interior pycnocline flow from the subtropical to the equatorial Pacific Ocean, *J. Phys. Oceanogr.*, *29*, 3073–3089, doi:10.1175/1520-0485(1999)029<3073:IPFFTS>2.0.CO;2.
- Johnson, G. C., and D. W. Moore (1997), The Pacific subsurface countercurrents and an inertial model, *J. Phys. Oceanogr.*, *27*, 2448–2459, doi:10.1175/1520-0485(1997)027<2448:TPSCAA>2.0.CO;2.
- Karnauskas, K. B., R. Murtugudde, and A. J. Busalacchi (2007), The effect of the Galápagos Islands on the equatorial Pacific cold tongue, *J. Phys. Oceanogr.*, *37*, 1266–1281, doi:10.1175/JPO3048.1.
- Kessler, W. S. (2006), The circulation of the eastern tropical Pacific: A review, *Prog. Oceanogr.*, *69*, 181–217, doi:10.1016/j.pocean.2006.03.009.
- Lavin, M. F., P. C. Fiedler, J. A. Amador, L. T. Ballace, J. Farber-Lorda, and A. M. Mestas-Núñez (2006), A review of eastern tropical Pacific oceanography: Summary, *Prog. Oceanogr.*, *69*, 391–398, doi:10.1016/j.pocean.2006.03.005.
- Liu, W. T., W. Tang, and P. S. Polito (1998), NASA scatterometer provides global ocean-surface wind fields with more structures than numerical weather prediction, *Geophys. Res. Lett.*, *25*, 761–764, doi:10.1029/98GL00544.
- Lukas, R. (1986), The termination of the Equatorial Undercurrent in the eastern Pacific, *Prog. Oceanogr.*, *16*, 63–90, doi:10.1016/0079-6611(86)90007-8.
- Maeda, S., and R. Kishimoto (1970), Upwelling off the coast of Peru, *J. Oceanogr. Soc. Jpn.*, *26*(5), 300–309, doi:10.1007/BF02769471.
- McCreary, J. P. (1981), A linear stratified ocean model of the coastal undercurrent, *Philos. Trans. R. Soc. London A*, *302*, 385–413, doi:10.1098/rsta.1981.0176.
- McCreary, J. P., Jr., P. Lu, and Z. Yu (2002), Dynamics of the Pacific subsurface countercurrents, *J. Phys. Oceanogr.*, *32*(8), 2379–2404, doi:10.1175/1520-0485(2002)032<2379:DOTPSC>2.0.CO;2.
- McWilliams, J. C., and G. Danabasoglu (2002), Eulerian and eddy-induced meridional overturning circulation in the tropics, *J. Phys. Oceanogr.*, *32*, 2054–2071, doi:10.1175/1520-0485(2002)032<2054:EAEIMO>2.0.CO;2.
- Penven, P., J. Pasapera, J. Tam, and C. Roy (2003), Modeling the Peru upwelling system seasonal dynamics, *GLOBEC Int. Newsl.*, *9*(2), 23–25.
- Penven, P., V. Echevin, J. Pasapera, F. Colas, and J. Tam (2005), Average circulation, seasonal cycle, and mesoscale dynamics of the Peru Current System: A modeling approach, *J. Geophys. Res.*, *110*, C10021, doi:10.1029/2005JC002945.
- Rowe, G. D., E. Firing, and G. C. Johnson (2000), Pacific equatorial subsurface countercurrent velocity, transport, and potential vorticity, *J. Phys. Oceanogr.*, *30*, 1172–1187, doi:10.1175/1520-0485(2000)030<1172:PESCVT>2.0.CO;2.
- Saunders, P. M., A. C. Coward, and B. A. De Cuevas (1999), Circulation of the Pacific Ocean seen in a global ocean model (OCCAM), *J. Geophys. Res.*, *104*, 18,281–18,299, doi:10.1029/1999JC900091.
- Shchepetkin, A. F., and J. C. McWilliams (2003), A method for computing horizontal pressure-gradient force in an ocean model with a nonaligned vertical coordinate, *J. Geophys. Res.*, *108*(C3), 3090, doi:10.1029/2001JC001047.
- Shchepetkin, A. F., and J. C. McWilliams (2005), The regional oceanic modeling system (ROMS): A split-explicit, free-surface, topography-following-coordinate oceanic model, *Ocean Modell.*, *9*, 347–404, doi:10.1016/j.ocemod.2004.08.002.
- Silva, N., and S. Neshyba (1979), On the southernmost extension of the Peru–Chile Undercurrent, *Deep Sea Res. Part A*, *26*, 1387–1393, doi:10.1016/0198-0149(79)90006-2.
- Silva, N., N. Rojas, and A. Fedele (2009), Water masses in the Humboldt Current System: Properties, distribution, and the nitrate deficit as a chemical water mass tracer for Equatorial Subsurface Water off Chile, *Deep Sea Res. Part II*, *56*, 1004–1020, doi:10.1016/j.dsr2.2008.12.013.
- Smith, W. H. F., and D. T. Sandwell (1997), Global seafloor topography from satellite altimetry and ship depth soundings, *Science*, *277*, 1956–1962, doi:10.1126/science.277.5334.1956.
- Steger, J. M., C. A. Collins, and P. C. Chu (1998), Circulation in the Archipelago de Colon (Galápagos Islands), November 1993, *Deep Sea Res. Part II*, *45*, 1093–1114, doi:10.1016/S0967-0645(98)00015-0.
- Strub, P. T., J. M. Mesias, V. Montecino, J. Rutllant, and S. Salinas (1998), Coastal ocean circulation off western South America, in *The Sea*, vol. 11, edited by A. R. Robinson and K. H. Brink, pp. 273–314, John Wiley, Hoboken, N. J.
- Toggweiler, J. R., K. Dixon, and W. S. Broecker (1991), The Peru upwelling and the ventilation of the South Pacific thermocline, *J. Geophys. Res.*, *96*, 20,467–20,497, doi:10.1029/91JC02063.
- Tsuchiya, M. (1975), Subsurface countercurrents in the eastern equatorial Pacific, *J. Mar. Res.*, *33*, suppl., 145–175.
- Tsuchiya, M. (1985), The subthermocline phosphate distribution and circulation in the far eastern equatorial Pacific Ocean, *Deep Sea Res. Part A*, *32*, 299–313, doi:10.1016/0198-0149(85)90081-0.
- Uppala, S. M., et al. (2005), The ERA-40 re-analysis, *Q. J. R. Meteorol. Soc.*, *131*, 2961–3012, doi:10.1256/qj.04.176.
- Wyrtki, K. (1963), The horizontal and vertical field of motion in the Peru Current, *Bull. Scripps Inst. Oceanogr.*, *8*, 313–344.
- Wyrtki, K. (1967), Circulation and water masses in the eastern equatorial Pacific Ocean, *Int. J. Oceanol. Limnol.*, *1*, 117–147.

X. Capet, Laboratoire de Physique des Océans, UMR 6523, UBO, CNRS, IFREMER, IRD, B.P. 70, Plouzane F-29280, France.

F. Colas, Institute of Geophysics and Planetary Physics, University of California, Los Angeles, Los Angeles, CA 90095-1567, USA.

I. Montes, Programa de Postgrado en Oceanografía, Departamento de Oceanografía, Universidad de Concepción, Barrio Universitario S/N, Cabina 5, Casilla 160-C, Concepcion, Chile. (ivonnem@udec.cl)

W. Schneider, Departamento de Oceanografía, Universidad de Concepción, Barrio Universitario S/N, Cabina 5, Casilla 160-C, Concepcion, Chile.